Engineering 20 (2023) 192–207

Contents lists available at ScienceDirect

Engineering

journal homepage: www.elsevier.com/locate/eng

Research
Civil Engineering—Article

Novel Radiation-Adjustable Heating Terminal Based on Flat Heat Pipe Combined with Air Source Heat Pump

Yifan Wu [a,b], Hongli Sun [a,b], Mengfan Duan [a,b], Borong Lin [a,b,*], Hengxin Zhao [a,b], Chaohung Liu [a,b]

[a] Department of Building Science, Tsinghua University, Beijing 100084, China
[b] Key Laboratory of Eco Planning and Green Building, Ministry of Education, Tsinghua University, Beijing 100084, China

ARTICLE INFO

Article history:
Received 10 May 2021
Revised 25 August 2021
Accepted 1 September 2021
Available online 04 January 2022

Keywords:
Novel heating terminal
Air-source heat pump
Structural improvement design
Maximum heating capacity
Rapid adjustability
Room temperature distribution

ABSTRACT

The electrification of building heating is an effective way to meet the global carbon target. As a clean and sustainable electrified heating technology, air-source heat pumps (ASHPs) are widely used in areas lacking central heating. However, as a major component of space heating, heating terminals might not fit well with ASHP in order to achieve both intermittency and comfort. Therefore, this study proposes a novel radiation-adjustable heating terminal combined with an ASHP to achieve electrification, intermittency, and better thermal comfort. Radiant terminals currently suffer from three major problems: limited maximum heating capacity, inability to freely adapt, and difficulty with combining them with ASHPs. These problems were solved by improving the structural design of the novel terminal (Improvement A–E). Results showed that the maximum heating capacity increased by 23.6% and radiation heat transfer ratio from 10.1% to 30.9% was provided for users with the novel terminal. Further, new flat heat pipe (FHP) design improved stability (compressor oil return), intermittency (refrigerant thermal inertia), and safety (refrigerant leakage risk) by reducing the length of exposed refrigerant pipes. Furthermore, a new phased operation strategy was proposed for the novel terminal, and the adjustability of the terminal was improved. The results can be used as reference information for decarbonizing buildings by electrifying heating terminals.

1. Introduction

Carbon emissions are being controlled globally to counter global warming. Buildings account for 30%–40% of global energy end-use [1]; CO_2 emissions from building operations reached 2.11 billion tonnes in China in 2019 [2]. Therefore, it is important to reduce the energy consumption of buildings, especially in relation to heating, in order to meet global carbon reduction targets [3].

Studies conducted in five high-income, high-emitting countries of Western Europe investigated household heat decarbonization and found that the concept of adopting low-carbon forms of space heating was extremely challenging for households because of different heating awareness, heating preferences, income, and culture [4]. Another study suggests that space heating accounts for a substantial portion of total energy consumption, and that heating systems offer a degree of flexibility in how they are used over time, which should be kept in mind when developing future energy systems to maintain a balance between supply and demand [5]. Some researchers have proposed that the comprehensive electrification of buildings would be an effective approach for achieving decarbonization of buildings, better utilizing renewable energy, and maintaining a balance between energy supply and demand [6,7]. In spite of the potential benefits of electrification of buildings, heating terminals, which is an important component of building space heating, have inherent problems associated with intermittency, comfort, and the prospect of electrification. Thus, the comprehensive electrification of buildings is challenging while maintaining thermal comfort, and it is imperative that both heating terminal problems are overcome and electrification is combined with heating terminals.

Radiators, floor heating, and fan coils are the most commonly employed traditional heating terminal types. Radiators and floor heating provide excellent thermal comfort, however, their adjustability for users is limited, making it difficult to adjust the heat load dynamically, and even though fan coils are highly variable, draughts and vertical temperature differences contribute to

* Corresponding author.
E-mail address: linbr@tsinghua.edu.cn (B. Lin).

https://doi.org/10.1016/j.eng.2021.09.019

thermal discomfort [8,9]. Attempts have been made by researchers to improve this traditional heating method. For example, Hu et al. [10] and Hemadri et al. [11] improved the radiator and fan coil designs by increasing the heat exchange area and adding materials that permitted a higher thermal conductivity; however, thermal comfort, even with the improved heat transfer capacity, was not improved. Wang et al. [12] proposed overhead floor heating to improve its adjustability but observed no visible improvement effects. As a result of the difference between convection and radiation heat transfer, intermittent and comfortable conditions are difficult to coexist for traditional heating terminals.

Although the above studies show that it is difficult to improve traditional heating terminals, studies have been conducted on developing new types of heating terminals combining the use of new materials and structures. In this regard, Chae and Strand [13] developed a new radiant system that incorporates a concentric tube heat exchanger (HE) embedded in a radiant panel. In addition, Li et al. [14] proposed a novel combined floor and Kang heating terminal. However, the position of the heating terminal was fixed, causing poor adjustability, so Li et al. [15] proposed a novel vertically adjustable radiant terminal that employed a modular design. Although this approach reduced the response time by more than 1.5 h, the heating capacity needed to be further improved. Based on floor heating, capillary tube heating has also been widely proposed for new terminal structures due to its flexibility and excellent thermal comfort; however, its low heating capacity (79.4–101.2 $W \cdot m^{-2}$) and poor adjustability (large thermal inertia of the wall) have limited its use [16,17]. The low heating capacity and the lack of rapid adjustability to changes in the indoor thermal load are two key problems that should be addressed in new terminals; although the above studies improved heat transfer, the extent of improvement was limited and the adjustability was poor.

Climate change action plans propose electric heating as a viable option and a low-carbon solution, which can be achieved through direct electrical heating or heat pumps [18–21]. Heat pumps are more efficient than direct electrical heating, and their lower carbon emissions make them an attractive choice [22]. Therefore, air-source heat pumps (ASHPs) are widely used as a clean, reliable, and sustainable heating technology in areas without central heating. The main types of ASHPs are air-to-water and air-to-air heat pumps [23]. Split air conditioners are common household heating terminals that incorporate air-to-air heat pumps and possess certain adjustability. However, the thermal comfort provided by them is especially poor, thus causing draughts and vertical temperature differences [24,25]. Therefore, ASHPs have recently been combined with novel heating terminals. For example, Shao et al. [26] produced a new refrigerant-heated radiator coupled with an ASHP; Dong et al. [27] studied a novel radiant-convective heating system based on an ASHP; Xu et al. [28] used heat pipes as heat radiators with an ASHP; Yang et al. [29] designed a multi-split ASHP unit; Zhang et al. [30] proposed a novel thermal storage refrigerant-heated radiator coupled with an ASHP.

While these novel heating terminals combined with ASHPs improved the thermal comfort and defrosting problems associated with traditional split air conditioners, such as those pertaining to the radiant-convective structure and thermal storage, some problems were evident, such as long exposed refrigerant pipes and large internal thermal resistance. Long exposed refrigerant pipes cause stability problems (compressor oil return), intermittency (refrigerant thermal inertia), and safety risks (risk of refrigerant pipe leakage). Therefore, considering the intermittency, comfort, and electrification requirements, as well as the inherent problems associated with newly designed terminals, the following three main problems must be addressed first with respect to the existing heating terminals:

- Problem 1 (P1): Maximum heating capacity of the terminal (especially the radiant terminal) is limited.
- Problem 2 (P2): Poor adjustment of the terminal in response to changes in the indoor thermal load.
- Problem 3 (P3): Combining terminals with sources (especially ASHPs) requires improvement.

In order to resolve these issues, we propose a novel heating terminal structure combining flat heat pipes (FHPs) and an ASHP to achieve adjustable radiation heating. FHPs are thin components that offer excellent heat transfer capacity. They have been widely used in heating, cooling, and dehumidification systems [31–39], as shown in Table 1 and Fig. 1.

Table 1 shows that FHPs can be used in solar energy, waste heat recovery, and electronic cooling systems owing to their excellent heat transfer capacities and thin physical dimensions. They are often used in small spaces [35]; however, their heating capacity is limited in large spaces [36], and the heating terminal structure needs to be improved before they can be used to heat large spaces.

Therefore, a novel radiation-adjustable heating terminal based on an FHP combined with an ASHP is proposed. The novel heating terminal broadens the range of heating capacity, improves the adjustability of the terminal, and facilitates the combination with ASHPs. These characteristics are achieved through the use of an FHP, the optimization of internal thermal resistance, and the addition of forced convection. In addition, a new phased operation strategy for the novel terminal is proposed, and the ability of users to adjust the terminal is further strengthened. The design presented here can be used to build the foundation for electrification of heating terminals to enable buildings to become carbon neutral by combining part-time and part-space heating.

2. Material and methods

2.1. Improved structural design of the novel terminal

Fig. 2 shows the improved structural design (Improvements A–E) and actual product of the novel terminal.

The novel terminal was improved in five ways (Improvements A–E) in this study as follows:

(1) Improvement A (Imp A): adding fins. The main aim of adding fins is to enhance the maximum heating capacity of the novel terminal. The heat exchange area of the terminal is increased by welding fins to its back. Each fin measures 10 cm in height, 0.5 mm in thickness, and 5.5 mm in spacing, respectively.

(2) Improvement B (Imp B): adding cross-flow fans. The addition of cross-flow fans to forced convection systems increases the maximum heat output and allows users to adjust the forced convection wind speed to the indoor thermal load. With the addition of the fan, both sides of the terminal are sealed to form an enclosed air duct. A cross-flow fan is preferred over an axial fan as it reduces noise as well as the air duct resistance. During the winter, cold air enters an indoor space through the air inlet of the cross-flow fan at the rear of the terminal when the rear cross-flow fan is running. The cold air is heated by fins inside the air duct, and the warm air is finally expelled through the air outlet beneath the terminal, which maintains a uniform indoor temperature. For space heating in winter, if the outlet is at a higher elevation, the buoyancy force in heating modes can cause significant "warm head and cold feet" with poor thermal comfort. Therefore, the terminal can be used for both heating and cooling. To prevent condensed water from flowing through both cross-flow fans and reducing their service life, both fans are arranged in the upper corner rather than the lower.

Table 1
Application of FHP in heating, cooling, and dehumidification.

Literature	Year	Application field	Image	Application effect
Wang et al. [31]	2021	Solar energy utilization	Fig. 1(a)	• A novel thermal storage solar air heater (TSSAH) with an FHP was proposed • Flat micro-heat pipe arrays (FMHPAs) performance exhibited excellent temperature uniformity during thermal discharge
Weng et al. [32]	2021	Data centre cooling and heat recovery	Fig. 1(b)	• The FHP realized the long-distance heat removal from the inside of the data cabinet to the outside • The instantaneous heat recovery efficiency of the micro-channel flat loop heat pipe heat recovery system was maintained within 81%–94%
Jouhara et al. [33]	2017	Waste heat recovery in the steel industry	Fig. 1(c)	• The rate of heat recovery during laboratory tests achieved by the FHP was about 5000 W • The application potential of FHPs for waste heat recovery in the steel industry was positive
Tan and Zhang [34]	2016	Building envelope	Fig. 1(d)	• The average heat transfer coefficient of the wall implanted with heat pipes reached 1.24 $W·m^{-2}·K^{-1}$ • Walls implanted with heat pipes saved a considerable amount of energy savings during the heating season
Xin et al. [35]	2018	Electronic cooling	Fig. 1(e)	• Heat pipes with a high heat transfer performance solved the problem associated with thermally controlling electronic devices • A slope-type wall was designed with grooves at the vapor–liquid interface in the heat pipe
Sun et al. [36]	2020	Space heating and cooling	Fig. 1(f)	• An FHP for heating and cooling showed a high heat response speed (180–465 s) • An FHP for heating and cooling showed high thermal uniformity (1.4 $°C·m^{-1}$)
Li et al. [37]	2021	High power telecommunication equipment cooling	Fig. 1(g)	• An FHP could work well in the vertical or horizontal position for high-power telecommunication equipment cooling • The highest thermal conductivity of the FHP was about 11 500 $W·m^{-1}·K^{-1}$
Wu et al. [38]	2021	Dehumidification	Fig. 1(h)	• Using an FHP for sensible heat transfer only and an HE for both cooling and dehumidification • Forced convection simultaneously increased the surface temperature (4–6 °C) and cooling capacity (75.7%)
Song et al. [39]	2021	Heat pump	Fig. 1(i)	• To achieve a high heat flow density, an FHP was used to collect heat in a condenser • The novel heat pump with the FHP increased the total exergy efficiency by 6.02%

(3) Improvement C (Imp C): double flow channels. These provide an increase in the heat exchange area and increase the maximum heating capacity. Considering the operating principle of an FHP, the upper and lower channels work with the FHP for cooling and heating, making it possible to use the novel terminal both in summer and winter in the future.

(4) Improvement D (Imp D): drilling the HE for the refrigerant. A refrigerant channel is formed by punching holes inside the heat exchanger. This combines the terminal with ASHP more skillfully and reduces the internal thermal resistance of the terminal. The heat exchanger consists of a copper plate having length, height, and thickness of 97 cm, 15 cm, and 10 mm, respectively. The copper plate is drilled with 6 mm diameter holes. The refrigerant channel spacing is 12 mm after drilling, and the outer side of each hole is connected by a matching U-bend to form a closed terminal-side refrigerant channel.

(5) Improvement E (Imp E): FHP for transferring heat. Using silicon grease, the FHP is bonded to the HE (surface without fins). The FHP is the key component that joins the terminal to the ASHP, and the flat surface of the HE fits well with the thin structure of the FHP. For space heating in winter, the internal working medium of the lower HE evaporates and the heat is transferred into the room via the upper HE. After condensing and releasing heat, the working medium returns to the part attached to the HE as a liquid where it again absorbs heat from the HE. The FHP used for transferring heat minimizes the problem associated with the long and exposed refrigerant pipes of existing terminals combined with an ASHP.

Fig. 3 illustrates the relationship between each of the improved structural designs and the problems associated with the existing heating terminals. It is noteworthy that no direct connection exists between the improved structural designs and the individual problems. For example, the addition of a cross-flow fan strengthens both the heating capacity and rapid adjustability. Similarly, drilling holes in the HE for refrigerant flow increases the heating capacity and improves the connection between the ASHP and heating terminal.

2.2. Experimental system

An innovative indoor heating system has been developed in a laboratory to allow manual control of the temperature. Considering the actual size of rooms in small homes and offices, the laboratory measures 3 m × 3 m × 3 m, and the southern exterior wall of the laboratory has a 2 m × 2 m window. The thermal parameters of the building envelope are as follows: exterior wall (K = 0.9 $W·m^{-2}·K^{-1}$, C = 1.05 $kJ·kg^{-1}·K^{-1}$), roof (K = 0.5 $W·m^{-2}·K^{-1}$, C = 0.75 $kJ·kg^{-1}·K^{-1}$), and exterior window (K = 2.8 $W·m^{-2}·K^{-1}$). K and C are the heat transfer coefficient and the specific heat capacity of building envelope, respectively. The airtightness of the laboratory is measured as 0.5 h^{-1} using the tracer gas method. Fig. 4 shows a schematic of the experimental system, which consists of an indoor heating terminal, an outdoor unit, connected pipes, and measuring instruments. For the indoor terminal, the lower part of the FHP, which acts as an evaporation section, is heated by the heat source, and the other part of the FHP, which acts as a condensation section, is heated by the principle of the heat pipe. The FHP was filled with a certain amount of acetone as the working fluid after it is vacuumed to 50% vacuum degree, and the filling rate is designed at approximately 20% in accordance with engineering experience. The total size of the FHP is 0.98 m × 0.88 m. The surface of the FHP is coated with a layer of Teflon (emissivity: 0.95) to increase the surface emissivity and enhance the heating capacity of the terminal. A

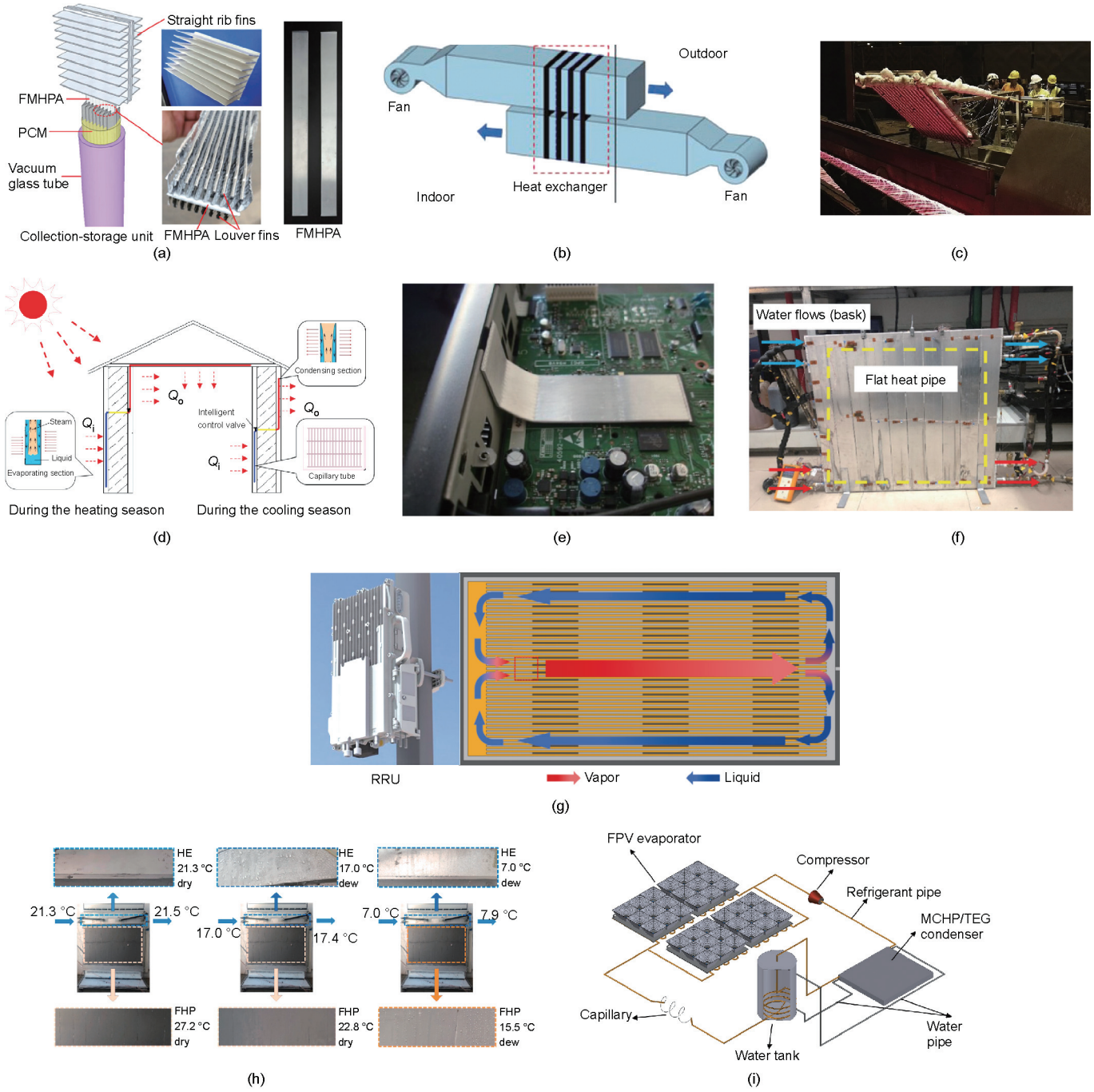

Fig. 1. Application of FHP in heating, cooling, and dehumidification: (a) solar energy utilization; (b) data center cooling and heat recovery; (c) waste heat recovery in the steel industry; (d) building envelope; (e) electronic cooling; (f) space heating and cooling; (g) high power telecommunication equipment cooling; (h) dehumidification; (i) heat pump. PCM: Q_i: inlet heat of heat pipe; Q_o: outlet heat of heat pipe; phase change material; FPV: fresnel concentration photovoltaic; RRU: remote radio unit; MCHP: micro-channel heat pipe; TEG: thermoelectric generator. Reproduced from Refs. [31–39] with permission.

description of the components used in the indoor and outdoor units is provided in Table 2.

A Coriolis mass flowmeter was placed on the measuring points to obtain the refrigerant flow rate, while temperature and pressure sensors are placed at the inlet and outlet of the evaporator and condenser, respectively. Fourteen thermocouples are arranged horizontally and vertically on the front surface of the FHP to obtain the surface temperature, and four thermocouples are provided at the top and bottom of the fins attached to the HEs, respectively. Three thermocouples are positioned at the inlet, outlet, and air duct to determine the mean air temperature at these three locations. In addition, nineteen thermocouples are placed in the laboratory space to obtain the mean ambient temperature, and six thermocouples are placed on the inner surfaces of the building envelope, as shown in Fig. 5. The sensor probe is made from low-emissivity metal, so the radiation effect is minimal. The temperature and pressure sensors transmit the data to a computer through a data acquisition system with an acquisition frequency of 10 s. All thermodynamic and thermophysical properties are calculated using REFPROP software.

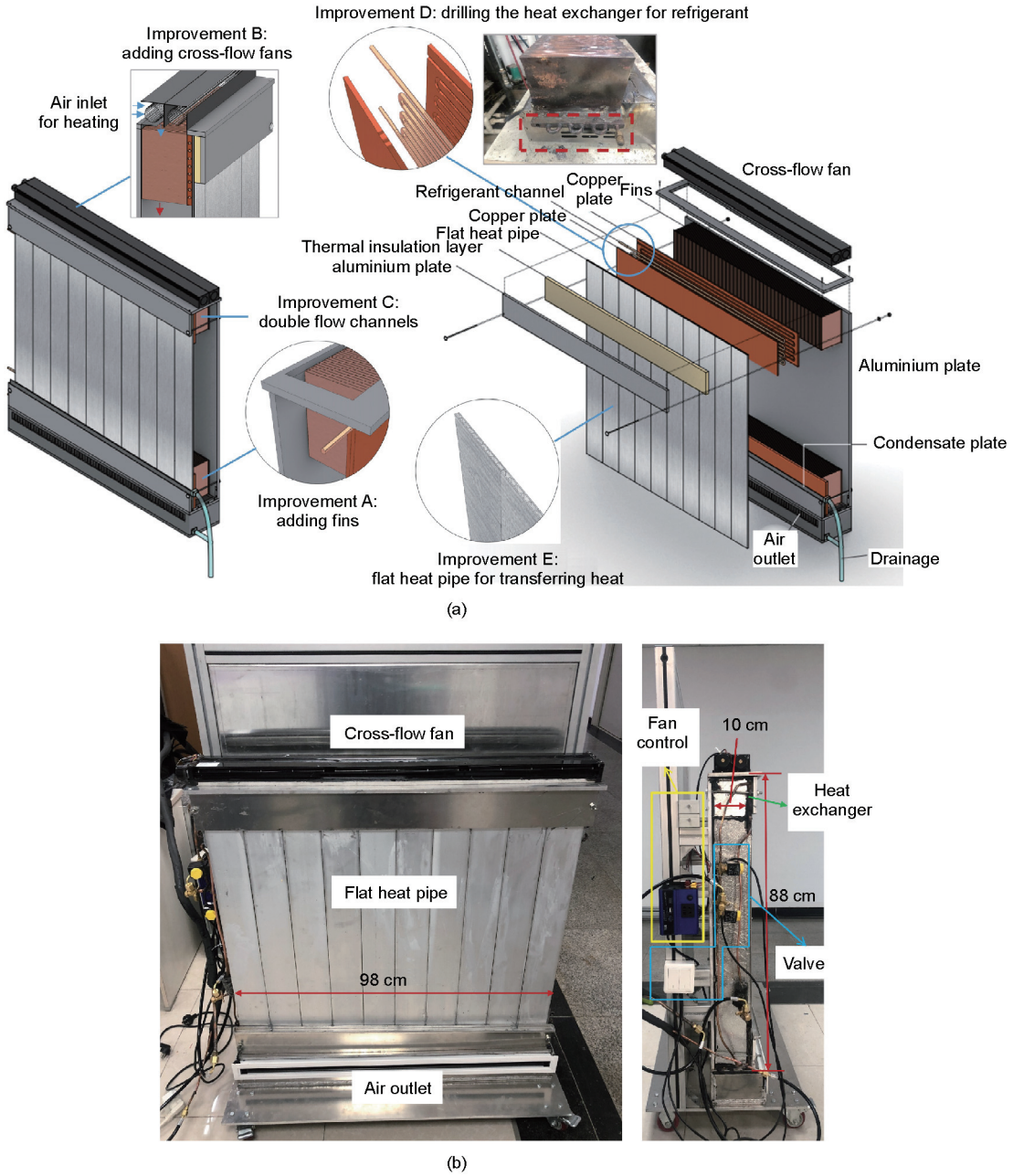

Fig. 2. Novel terminal: (a) improved structural design of the novel terminal and (b) actual novel terminal.

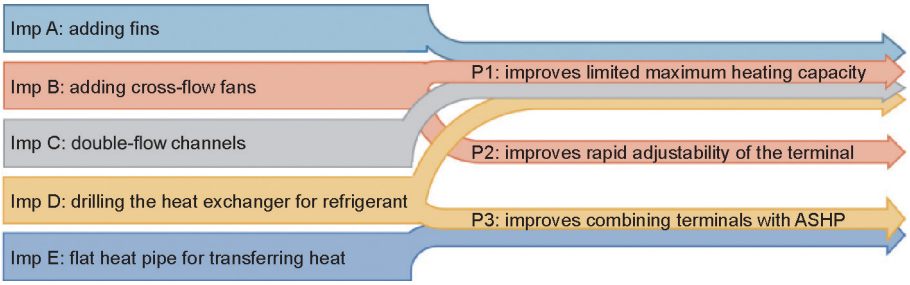

Fig. 3. Schematic diagram of improvement in relation to problems with existing terminals.

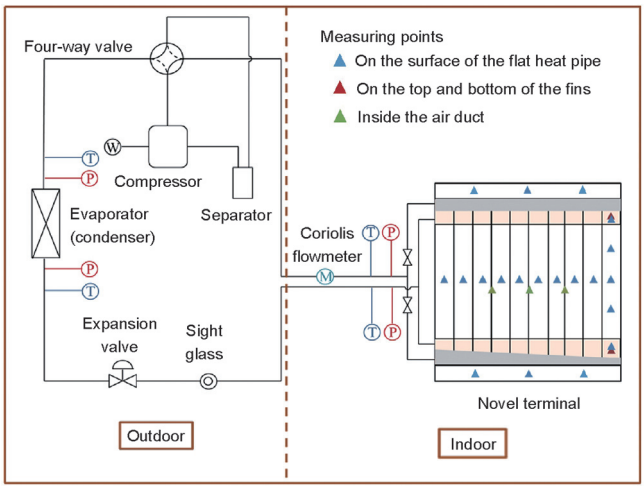

Fig. 4. Schematic of the experimental system.

Table 2
Description of components used in the indoor terminal and outdoor unit of the experimental system.

Location	Component	Description
Indoor terminal	HE	Material: copper Size: 97 cm × 15 cm × 10 mm ($L \times H \times W$), 2 pieces Inner hole diameter: 6 mm Pipe spacing: 12 mm
	FHP	Material: aluminum Size: 9.8 cm × 88 cm × 0.5 cm ($L \times H \times W$), 10 pieces Charge: acetone (filling rate: 20%) Surface: teflon spray (emissivity: 0.95) Connection with HE: silicon grease
	Fins	Material: copper Size: 15 cm × 10 cm × 0.5 mm ($L \times H \times W$), 150 pieces Fin spacing: 5.5 mm Connection with HE: welding
	Fans	Type: cross-flow fan Size: 105 cm × 5 cm × 5 cm, length of air inlet 98.6 cm Speed: 0–2400 r·min^{-1} Air volume: 0–450 m^3·h^{-1} Sound: 32 dB
	Air outlet	Size: 98 cm × 6.5 cm ($L \times H$)
Outdoor unit	Compressor	Type: hermetic rotary vertical single-cylinder motor compressor (QX-B146C030A) Displacement: 14.6 cm^3 Nominal heating capacity: 2100 W
	Refrigerant	Type: R22 Charge: 0.90 kg
	HE	Copper pipe: length, external diameter, inner diameter of 36.4 m, 7 mm, and 6 mm, respectively Pipe spacing: 20 mm Path: 2 Fin thickness: 0.1 mm Fin spacing:1.8 mm

L: length; *H*: height; *W*: width.

2.3. Experimental conditions

By improving the structure of the novel heating terminal, three heating modes are obtained: Mode 1, Mode 2, and Mode 3 (as shown in Fig. 6). Solenoid valves are arranged in the upper and lower channels. Mode 1 is the most basic mode of operation without forced convection. Solenoid valves regulate the opening and closing of the refrigerant channel in the lower and upper HEs. At this point, most of the heat is produced through radiant heating, but a certain amount of it is also transferred by natural convection. In Mode 2, the cross-flow fan is operated at maximum wind speed, in which the forced convection heat transfer of the fins inside the air duct is supplemented. In this case, forced convection heat transfer is added by radiation and natural convection. Mode 3 is further developed as an extension of Mode 2. In Mode 3, the cross-flow fan runs at the maximum wind speed, and the refrigerant channels of both the upper and lower HEs are opened simultaneously via valve control.

For different modes, the heating capacity, radiation heat transfer ratio, and rise in ambient temperature are determined. Temperature control of (20.0 ± 0.5) °C is used to obtain the heating capacity and radiation heat transfer ratio. This ensures that the experiment is carried out objectively and accurately. To evaluate the heat transfer characteristics, the heating capacity Q is defined as follows:

$$Q = G(h_i - h_o) \times 1000/3600 \tag{1}$$

where G is the flow rate of refrigerant (kg·h^{-1}); h_i and h_o are the inlet and outlet enthalpy of terminal (kJ·kg^{-1}).

The radiation heating capacity Q_r and the convection heating capacity Q_c of the terminal are also determined. Q_r is calculated using the mean radiant temperature (MRT) method:

$$Q_r = \varepsilon A \sigma_b \left(T_s^4 - \mathrm{MRT}^4\right) \tag{2}$$

where ε is the surface emissivity; A represents the surface area of radiant panel (m^2); σ_b is the Stefan–Boltzmann constant, 5.67 × 10^{-8} W·m^{-2}·K^{-4}; T_s is the surface temperature of terminal (K); MRT represents the mean radiant temperature (K). And Q_c is calculated as the sum of the forced convection heating capacity Q_f and the natural convection heating capacity Q_n:

$$Q_f = c\rho V(T_o - T_i) \tag{3}$$

The natural convection heating capacity Q_n can be calculated using the expression of natural convection in an infinite space. The Nusselt Nu and Grashof Gr numbers can be expressed as follows:

$$Nu = \gamma(Gr \cdot Pr)^n = \gamma \cdot Ra^n \tag{4}$$

$$Gr = g\alpha(T_s - T_a)l^3/\nu^2 \tag{5}$$

where c is the heat capacity of air, 1005 J·kg^{-1}·K^{-1}; ρ is the density of air (kg·m^{-3}); V represents the velocity of air in forced convection (m^3·s^{-1}); γ and n are coefficients for different flow and heat transfer conditions, which can be obtained by looking up the table of empirical formulas; Pr is Prandtl number and Ra is Rayleigh number; g is the gravitational acceleration (m·s^{-2}); α is the volume expansion coefficient (K^{-1}); l represents the characteristic length (m); ν is the kinematic viscosity (m^2·s^{-1}); T_i, T_o, T_s are the inlet, outlet, and surface temperatures of the terminal, respectively, and T_a is the ambient temperature (°C).

Therefore, Q_n and Q_c can be expressed as

$$Nu = K_n l/\lambda \tag{6}$$

$$Q_n = K_n A(T_s - T_a) \tag{7}$$

$$Q_c = Q_f + Q_n \tag{8}$$

where K_n is the natural convection heat transfer coefficient (W·m^{-2}·K^{-1}); λ is the thermal conductivity of air (W·m^{-1}·K^{-1}).

The radiation heat transfer ratio β, can be expressed as

$$\beta = Q_r/Q \times 100\% \tag{9}$$

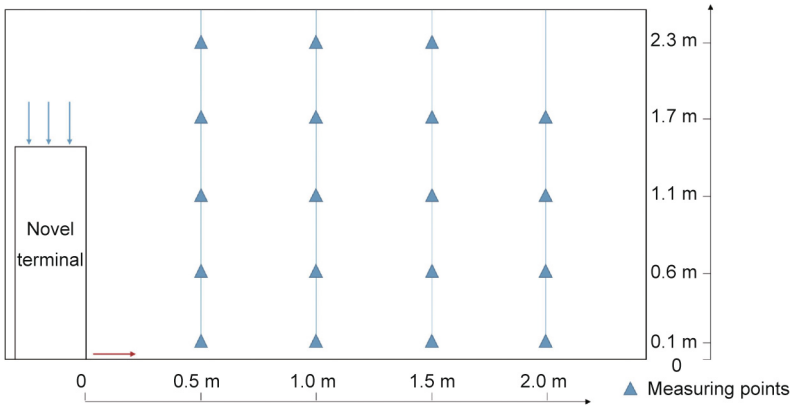

Fig. 5. Schematic of measuring points within the laboratory.

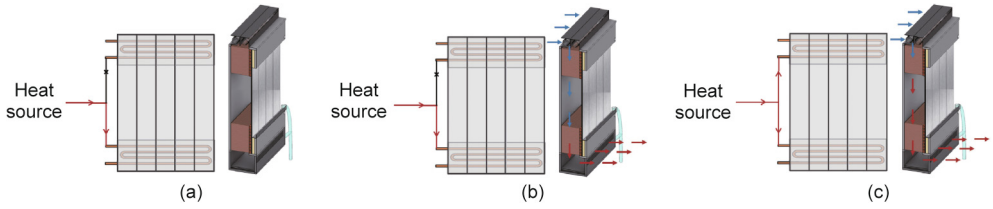

Fig. 6. Three heating modes provided by the novel terminal: (a) Mode 1, (b) Mode 2, and (c) Mode 3.

Accordingly, heat transfer from the source to the terminal Q is compared with heat transfer from the terminal to the room $Q_r + Q_c$ to verify the accuracy of the experimental results, as discussed in Section 4.5.

To ensure the objectivity and accuracy of the experimental results, the initial indoor temperature in the three operating modes is controlled to 7–8 °C when the outside temperature was 1–2 °C. In order to compare and analyze the rise in ambient temperature, we studied variations in the indoor average temperature with time for the three types of operations.

Furthermore, the heating capacity and room temperature distribution are explored under different forced convection wind speeds, with the room temperature is also controlled to be approximately 20 °C to ensure objective and accurate experimental results. Initially, the outlet wind speeds of the terminal are controlled at 2.0, 1.5, 1.0, 0.5, and 0 $m \cdot s^{-1}$ corresponding to the air volume flow rates of 458.6, 344.0, 229.3, 114.7 and 0 $m^3 \cdot h^{-1}$ by a rotary knob to calibrate the basic operating conditions of a cross-flow fan. An analysis is then conducted under these operating conditions.

2.4. Experimental instruments

Table 3 and Fig. 7 summarize the experimental instruments used to measure different parameters, such as surface temperature, inlet and outlet air temperature, and flow rate.

3. Results

3.1. Solving problem 1: Improving the maximum heating capacity

The heating capacity of the novel terminal in Modes 1, 2, and 3 is shown in Fig. 8. The results showed that the maximum heating capacity of the terminal increased from 1649.9 W in Mode 1 to 2039.6 W in Mode 2 by the addition of fins (Opt A) and cross-flow fan (Opt B). The outdoor temperature during operation (1–2 °C) is lower than that corresponding to nominal heating capacity (5–7 °C), so the maximum heating capacity is less than the nominal heating capacity (2100 W). The heating capacity increased by 389.7 W, which is 23.6% higher than that of Mode 1. However, the double-flow channels (Opt C) failed to achieve the expected effect, and Mode 3 provided a lower heating capacity than Mode 2.

There are two limitations to Opt C is limited in two ways: The maximum heating capacity of the terminal is limited by the compressor and the operating state of the FHP affects the double-flow channels. Mode 2 has only the lower HE running and the FHP is operating normally (lower: evaporator; and upper: condenser). However, in Mode 3, the simultaneous operation of the upper and lower HEs affected the normal operating state of the FHP to a certain extent.

A comparison between the space heating capabilities of the novel heating terminal and the conventional FHP is shown in Fig. 9 at the same indoor temperature of 20 °C. The conventional terminal is composed of FHPs, hot water pipes without fins, fans, drilled HEs, and

Table 3
Specifications of experimental instruments.

Instrument	Image	Measured data	Unit	Accuracy
T-type thermocouple	Fig. 7(a)	Surface temperature and ambient temperature	°C	±0.050
Pressure transmitter (MIK-P300)	Fig. 7(b)	Inlet and outlet pressure of condenser and evaporator	MPa	±0.006
Anemometer (TJHY FB-1A)	Fig. 7(c)	Outlet wind speed	$m \cdot s^{-1}$	±0.050
Coriolis mass flowmeter	Fig. 7(d)	Flow rate	$kg \cdot h^{-1}$	±0.005
Electric power data logger (WGLZY-1)	Fig. 7(e)	Electric power of outdoor unit and fans	W	±2%
Infrared imager (TESTO-875)	Fig. 7(f)	Infrared images	—	Calibrated by measured temperature

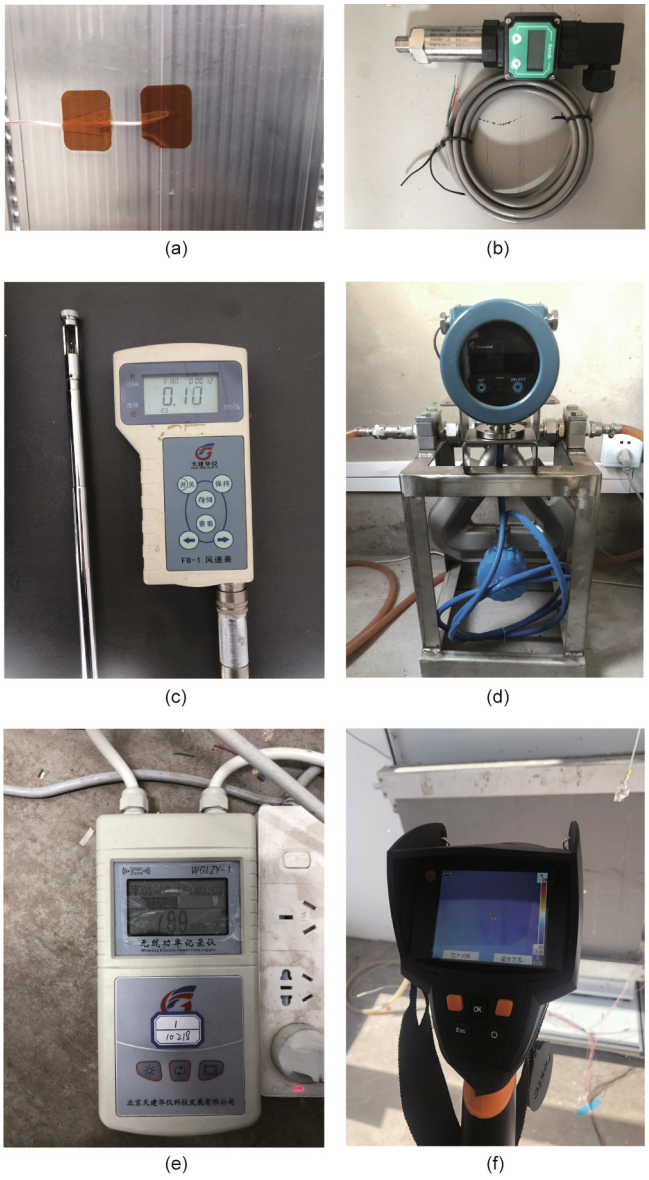

Fig. 7. Specifications of experimental instruments: (a) T-type thermocouple; (b) pressure transmitter; (c) anemometer; (d) coriolis mass flowmeter; (e) electric power data logger; and (f) infrared imager.

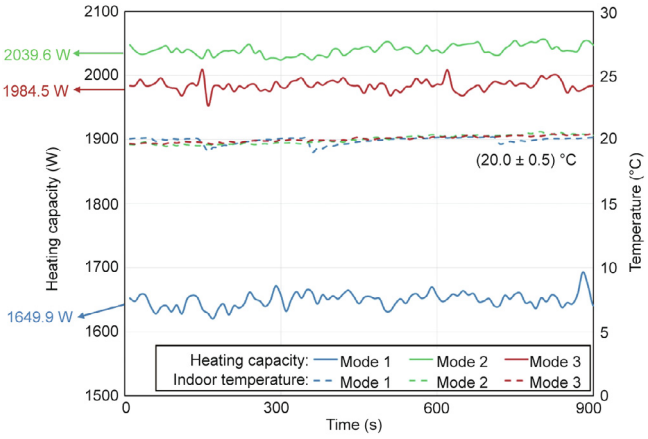

Fig. 8. Heating capacity under different operating modes.

other improved structural designs [36]. The novel terminal is upgraded with an air source heat pump with refrigerant R22, while the conventional terminal uses water as a working medium at different temperatures (40/50/60/70 °C). In order to strengthen the heating capacity, fans, fins, and forced convection air duct are added at the rear of the novel terminal. Both terminals use FHPs with the same area and the same internal working medium. The results showed that the heating capacity of the novel terminal (Mode 2) increased by 1194.6 W which is 2.4 times that of the maximum heating capacity of the conventional terminal (heat source at 70 °C). An increase in the heating capacity at 40 °C is found to be 1718.6 W which is 6.4 times that of a conventional terminal. It can be seen that the improved structural design by adding fins (Opt A), adding cross-flow fans (Opt B), and drilling the HE for refrigerant (Opt D) considerably enhanced the heating capacity of the terminal (Problem 1).

3.2. Solving problem 2: Improving the dynamic adjustable ability

The thermal response speed and radiation heat transfer ratio are crucial indicators of dynamic adjustment. The thermal response speed reflects the ability of the terminal to dynamically adjust. In this respect, it is only possible to achieve a dynamic adjustment effect through the terminal if the thermal response is fast enough. The radiation heat transfer ratio measures a system's specific dynamic adjustable performance. Users can select an appropriate radiation heat transfer ratio by adjusting different modes. Generally, the thermal comfort is enhanced when the radiation heat transfer ratio is higher; however, the heating capacity is enhanced when the convection heat transfer ratio is higher.

Fig. 10 shows the thermal response speeds in Modes 1, 2, and 3. The results show that an increase in forced convection from Mode 1 to Mode 2 reduces the time required to raise the indoor temperature from 7–8 to 18 °C by 3060 s. Under Opt B (the addition of cross-flow fans), the thermal response of the room is 44% faster, allowing for greater dynamic adjustment of the terminal (Problem 2).

Fig. 11 shows the radiation heat transfer ratios in Modes 1, 2, and 3. The results show that the users could adjust the radiation heat transfer ratios of the novel terminal from 10.1% to 26.5%. The radiation heat transfer ratio is enhanced by 2.6 times, implying better dynamic adaptability of the terminal (Problem 2).

3.3. Solving problem 3: Improving the combination of the heating terminal and ASHP

System operation must be stable when combining the terminal with an ASHP. In Table 4, Mode 3 is used as an example to illustrate

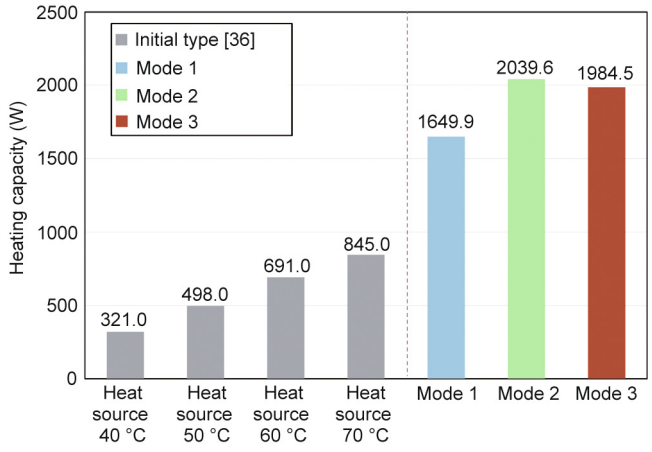

Fig. 9. Comparison between space heating capabilities of novel terminal and an initial FHP terminal type.

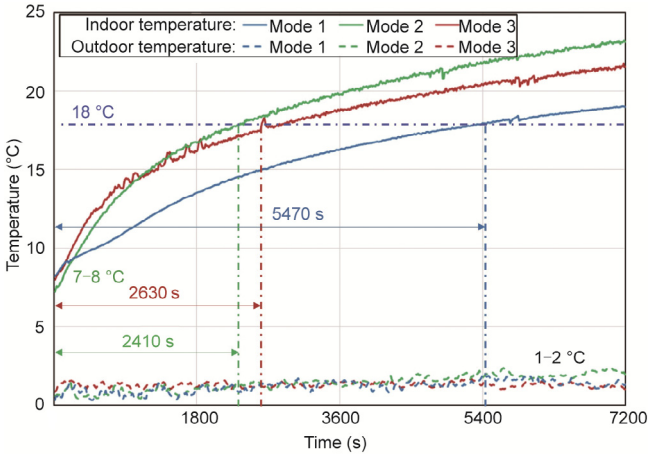

Fig. 10. Thermal response speeds: rise in ambient temperature under different operational modes.

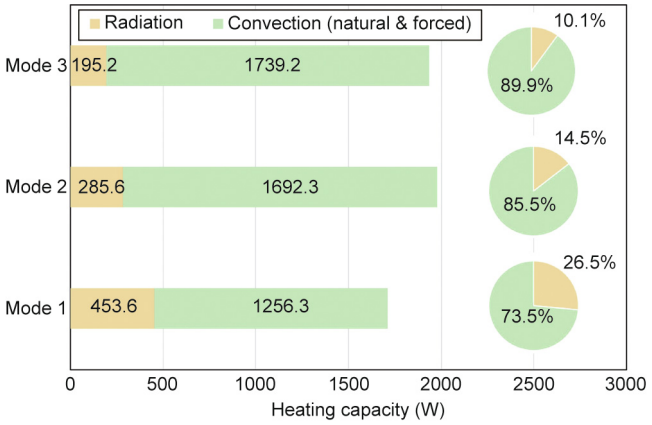

Fig. 11. Radiation heat transfer ratio: radiation and convection under different operating modes.

the changes in the key parameters such as the thermophysical parameters of the inlet and outlet, exhaust temperature of the compressor, and flow rate of the refrigerant for 3 min duration under stable conditions. By using a drilled HE (Opt D) and FHP (Opt E), the cooling system and heating terminal are optimized structurally, ensuring a more stable operation. It is noteworthy that both the compressor and the fan consume electric power; therefore, the energy efficiency ratio (EER) can be used to measure energy efficiency. The electric power of the cross-flow fan is also considered, although the maximum measured electric power is only 13.4 W. Table 5 lists the key parameters of the three operational modes under stable conditions. Fig. 12 shows the pressure-enthalpy diagram corresponding to the operational conditions for the three modes.

A stable operation can be achieved in all three operating modes. The inlet and outlet pressures of the terminal in the three modes are 3.2–2.9, 2.8–2.5, and 2.2–2.1 MPa, respectively, while the refrigerant flow rates are maintained in the range of 41.8–45.9 $kg{\cdot}h^{-1}$, with an EER of 1.5, 1.9, and 2.2, respectively. The inlet and outlet pressures in Modes 1 and 2 are higher than normally observed with R22, while Mode 3 operates in the typical range of 1.8–2.2 MPa. The higher temperatures and pressures of Modes 1 and 2 are related to the outdoor unit, which is limited by a fixed-speed compressor. Also, the opening of the expansion valve affected the performance in Modes 1 and 2. These performances may be improved by integrating a variable-speed compressor in the future. However, the primary focus of this study is not the heat source temperature. The most important aspect of the terminal is its capability of being adjusted, including the dynamic and radiation properties, and these are discussed further in Sections 4.1 and 4.2. However, the three modes are generally found stable during the operation. The results show that the novel terminal is successfully combined with the ASHP to provide heat energy under stable operating conditions (Problem 3).

3.4. Improvement of the FHP used for transferring heat

The FHP used in the improved structural design for transferring heat in order to solve the three main problems associated with existing heating terminals is discussed in this section. Fig. 13 shows the schematic and actual diagram of the FHP used to transfer the heat energy. Heating terminals that have previously been combined with an ASHP [26,27] are generally radiant panels covered with refrigerant pipes. This type of terminal structure has a long and exposed refrigerant pipe, as shown in Fig. 13(a). In this study, the combination of the heating terminal and ASHP is improved. Using phase change, the FHP transfers heat instead of the long refrigerant pipe. Refrigerant pipes shall cover the back

Table 4
Novel terminal combined with ASHP under different conditions: Mode 3 for example (0–3 min).

Time (s)	T_i (°C)	P_i (MPa)	h_i ($kJ{\cdot}kg^{-1}$)	T_o (°C)	P_o (MPa)	h_o ($kJ{\cdot}kg^{-1}$)	T_{exh} (°C)	G ($kg{\cdot}h^{-1}$)	Q (W)	P (W)	EER
10	58.5	2.2	420.8	51.4	2.1	265.1	64.8	45.9	1983.8	883.9	2.2
20	58.7	2.2	421.0	51.4	2.1	265.2	64.9	45.8	1983.9	883.9	2.3
30	58.7	2.2	420.9	51.4	2.1	265.2	64.9	46.0	1991.1	883.9	2.3
40	58.5	2.2	420.6	51.4	2.1	265.2	65.0	45.9	1981.1	883.9	2.2
50	59.5	2.2	421.8	51.4	2.1	265.1	65.1	46.0	2003.1	883.9	2.3
60	58.8	2.2	420.9	51.4	2.1	265.1	65.2	45.9	1985.1	883.9	2.2
70	58.7	2.2	420.9	51.4	2.1	265.1	65.2	46.1	1994.6	883.9	2.3
80	58.8	2.2	420.9	51.4	2.1	265.1	65.3	46.2	1997.5	883.9	2.3
90	58.9	2.2	421.0	51.4	2.1	265.2	65.4	45.9	1987.2	883.9	2.2
100	58.9	2.2	421.1	51.4	2.1	265.2	65.4	45.4	1968.3	883.9	2.2
110	58.9	2.2	421.1	51.4	2.1	265.2	65.5	45.8	1981.1	883.9	2.2
120	58.7	2.2	420.8	51.4	2.1	265.2	65.5	45.8	1979.3	883.9	2.2
130	59.0	2.2	421.1	51.5	2.1	265.3	65.5	45.5	1971.1	883.9	2.2
140	58.9	2.2	421.1	51.5	2.1	265.3	65.6	45.7	1979.8	883.9	2.2
150	58.8	2.2	420.9	51.5	2.1	265.3	65.6	45.9	1984.1	883.9	2.2
160	58.0	2.2	420.0	51.5	2.1	265.3	65.7	45.9	1972.1	883.9	2.2
170	59.1	2.2	421.2	51.5	2.1	265.4	65.7	45.9	1987.5	883.9	2.2
180	59.1	2.2	421.1	51.6	2.1	265.4	65.7	46.1	1995.1	883.9	2.3

T_{exh}: exhaust temperature of compressor; P_i: inlet pressure of terminal; P_o: outlet pressure of terminal; P: total electric power of compressor and fan.

Table 5
Novel terminal combined with ASHP under different conditions: Mode 1, Mode 2, and Mode 3 (initial time).

Type	T_i (°C)	P_i (MPa)	h_i (kJ·kg^{-1})	T_o (°C)	P_o (MPa)	h_o (kJ·kg^{-1})	T_{exh} (°C)	G (kg·h^{-1})	Q (W)	P (W)	EER
Mode 1	79.8	3.2	425.3	63.8	2.9	282.9	96.7	41.8	1652.5	1108.1	1.5
Mode 2	82.6	2.8	436.1	56.3	2.5	272.0	98.0	45.0	2047.5	1070.6	1.9
Mode 3	58.5	2.2	420.8	51.4	2.1	265.1	64.8	45.9	1983.8	883.9	2.2

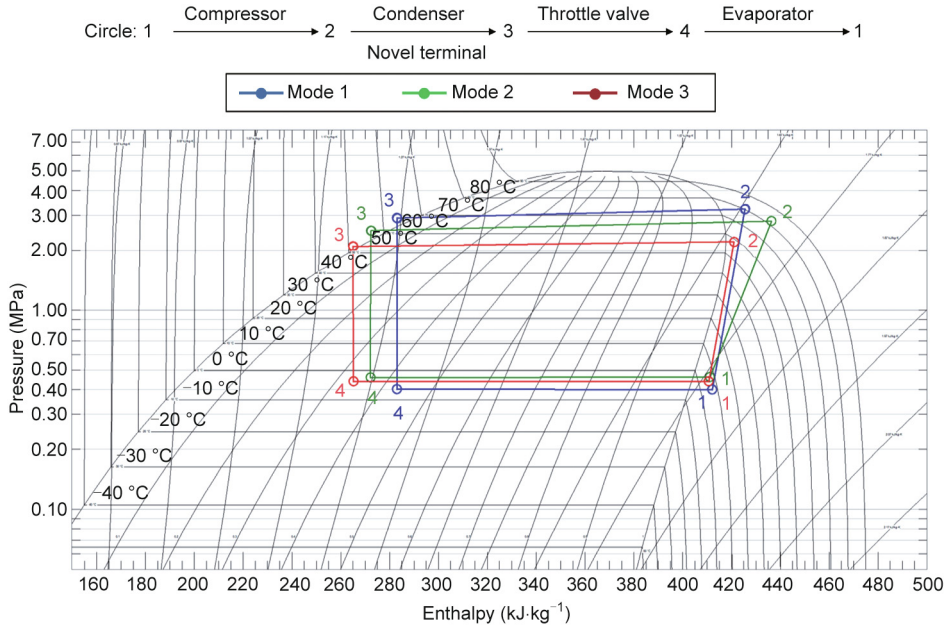

Fig. 12. Pressure–enthalpy diagram for the three modes in a stable stage. Point 2 shows the state point before entering the terminal, the compressor outlet state point is not shown in the circle.

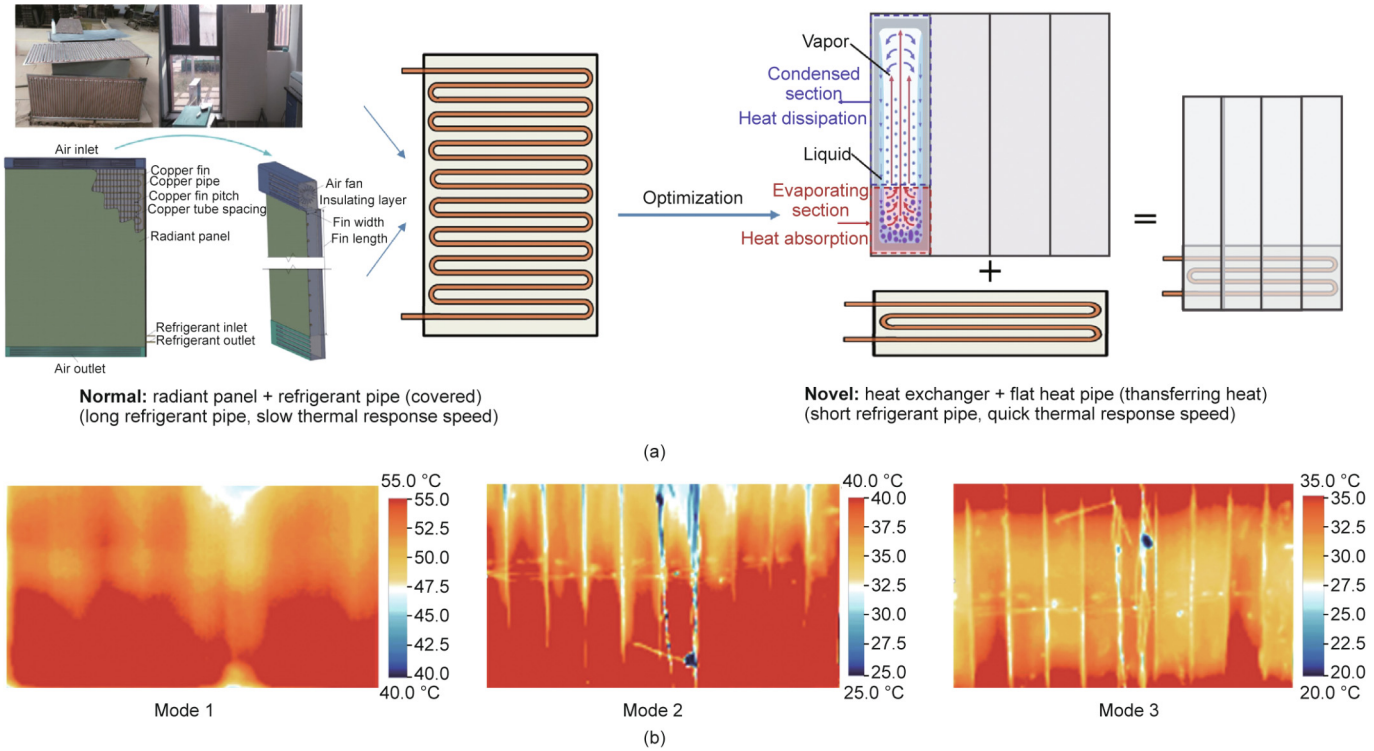

Fig. 13. FHP for transferring heat. (a) Schematic diagram and (b) actual images in different modes taken by the infrared imager.

of the terminal if FHPs are not used. As per the current terminal structure, the distance between pipes is 12 mm, and the height is 0.88 m. Thus, at least 70 refrigerant pipes should be arranged on the rear and their total length is around 68.6 m. However, if the FHP is used to transfer heat, only eight refrigerant pipes in the upper and lower HEs are required, which reduces the total length to 15.7 m. The application of an FHP reduces the total length by 52.9 m, which is only 22.9% of the refrigerant pipe. This novel terminal can be conceptualized as a small HE utilizing FHPs to transfer heat

The FHP is used to transfer heat (Opt E), which has a simplified terminal structure and provides the following advantages. ① As the terminal refrigerant pipe length is greatly reduced, the initial investment is lower and the safety of the terminal is enhanced, decreasing the risk of refrigerant leaking from the pipe behind the terminal. ② The operation of the system is improved. Reducing terminal refrigerant pipe length eliminates the problem of oil draining from the compressor and increases the compressor's thermal response. ③ Thermal comfort is enhanced. Although the temperature of the FHP is uniform, there is a difference in the surface temperature according to the three operational modes depicted in Fig. 13(b).

4. Discussion

4.1. Dynamic and adjustable novel terminal with phased operation strategy

To provide enhanced thermal performance, this study proposes a phased operation strategy for space heating based on the rapid adjustability of the terminal. The heating process can be mainly divided into two periods, the initial starting period (Mode 2) and subsequent stable period (improved Mode 1), as shown in Fig. 14. The maximum heating capacity is provided during the starting period to achieve a rapid thermal response, whereas, the high radiation heat transfer ratio is provided during the stable period to maintain thermal comfort.

During the initial heating period, the novel terminal uses forced convection to achieve its maximum heating capacity quickly, and thus achieves a fast thermal response. The experimental results reveal that the terminal provides a heating capacity of 2000 W during the initial heating period, and it takes 40 min to raise the indoor temperature from 8 to 18 °C. When the indoor temperature reaches 18 °C, it is within an acceptable temperature range for thermal comfort. Here, the focus is on achieving thermal comfort rather than rapid heating.

Thus, the operational mode of the terminal is changed to increase the radiation heat transfer ratio. The largest improvement in thermal comfort is achieved when the temperature in the experiment is maintained at 18–22 °C, and draughts are significantly reduced. Due to the excellent adjustability of the terminal, it has the capability to automatically adjust the temperature according to users' preferences (such as to 16, 18, or 20 °C, for example), thus improving its thermal performance for individual users.

4.2. Radiation-adjustable novel terminal with forced convection

Different forced convection wind speeds offer users a variety of adjustment options. Fig. 15 shows the heating capacity under different forced convection wind speeds. The results indicate a linear relationship between heating and outlet wind speed.

There are some differences between the calibrated outlet and actual outlet wind speeds during the experiment. For example, the outlet wind speed is calibrated as 2.0 $m{\cdot}s^{-1}$, but the experiments showed that the speed changed to 1.6 $m{\cdot}s^{-1}$ when the terminal is heated. When the terminal is calibrated, it is not heated. However, when it is heated in the actual experiment, an upward thermal buoyancy force is formed in the terminal's internal air duct, which reduces the outlet wind speed to a certain extent.

Fig. 16 shows the radiation heat transfer ratios corresponding to different outlet wind speeds. The results show that the radiation heat transfer ratio declined gradually with increasing forced convection wind speed and that it could be adjusted from 14.5% to 30.9%. The upper and lower air inlets and outlets of the terminal are completely sealed when conducting additional experiments. An additional experiment is necessary because the outlet wind speed of 0.3 $m{\cdot}s^{-1}$ exists in reverse without a cross-flow fan, namely it is caused by thermal buoyancy and the maximum radiation heat transfer ratio has been weakened. When the inlets and outlets are sealed completely, the radiation heat transfer is increased by 54.6 W and the ratio by 4.4%. The radiation heat transfer ratio reached 30.9%, which is acceptable for a heating terminal.

4.3. Room temperature distribution under forced convection

Fig. 17 demonstrates the differences in the room temperature distribution under different forced convection speeds. The vertical temperature difference and air supply distance are related to changes in temperature and wind speed recorded at the measuring points.

As shown in Fig. 17(a), the calibrated outlet wind speed is 2.0 $m{\cdot}s^{-1}$, but the actual outlet wind speed is 1.6 $m{\cdot}s^{-1}$. At this point, the air supply was approximately 1.5 m away from the

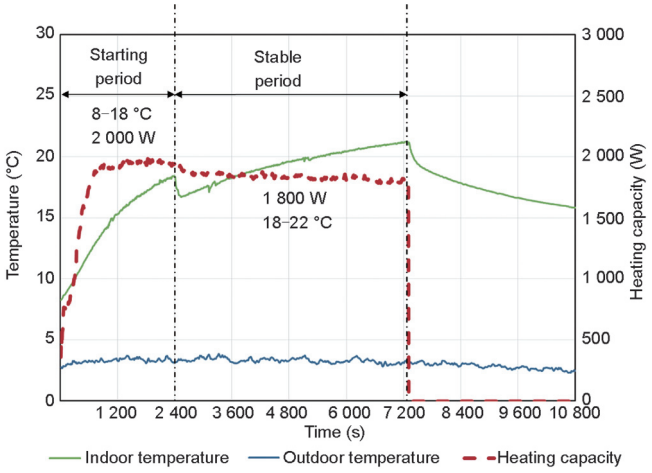

Fig. 14. Dynamic and adjustable phased operation strategy.

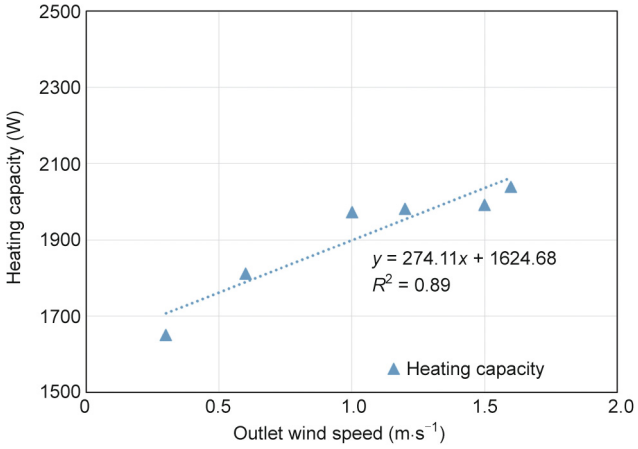

Fig. 15. Heating capacity under different forced convection wind speeds.

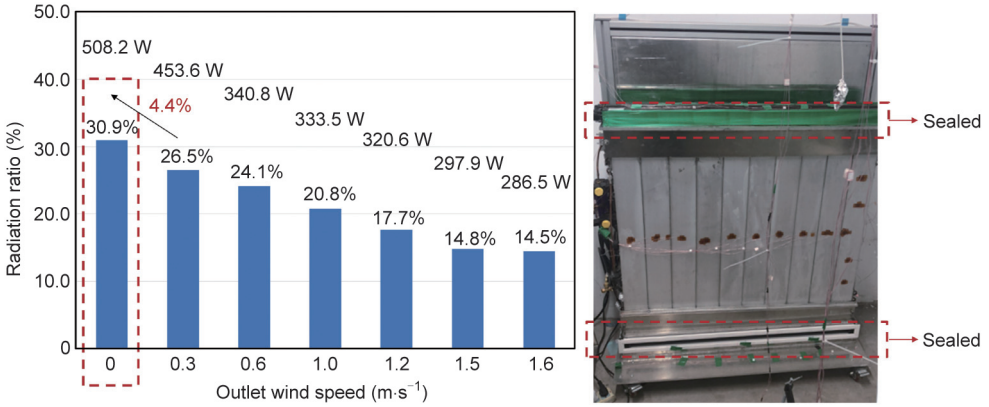

Fig. 16. Radiation heat transfer ratio under different forced convection wind speeds.

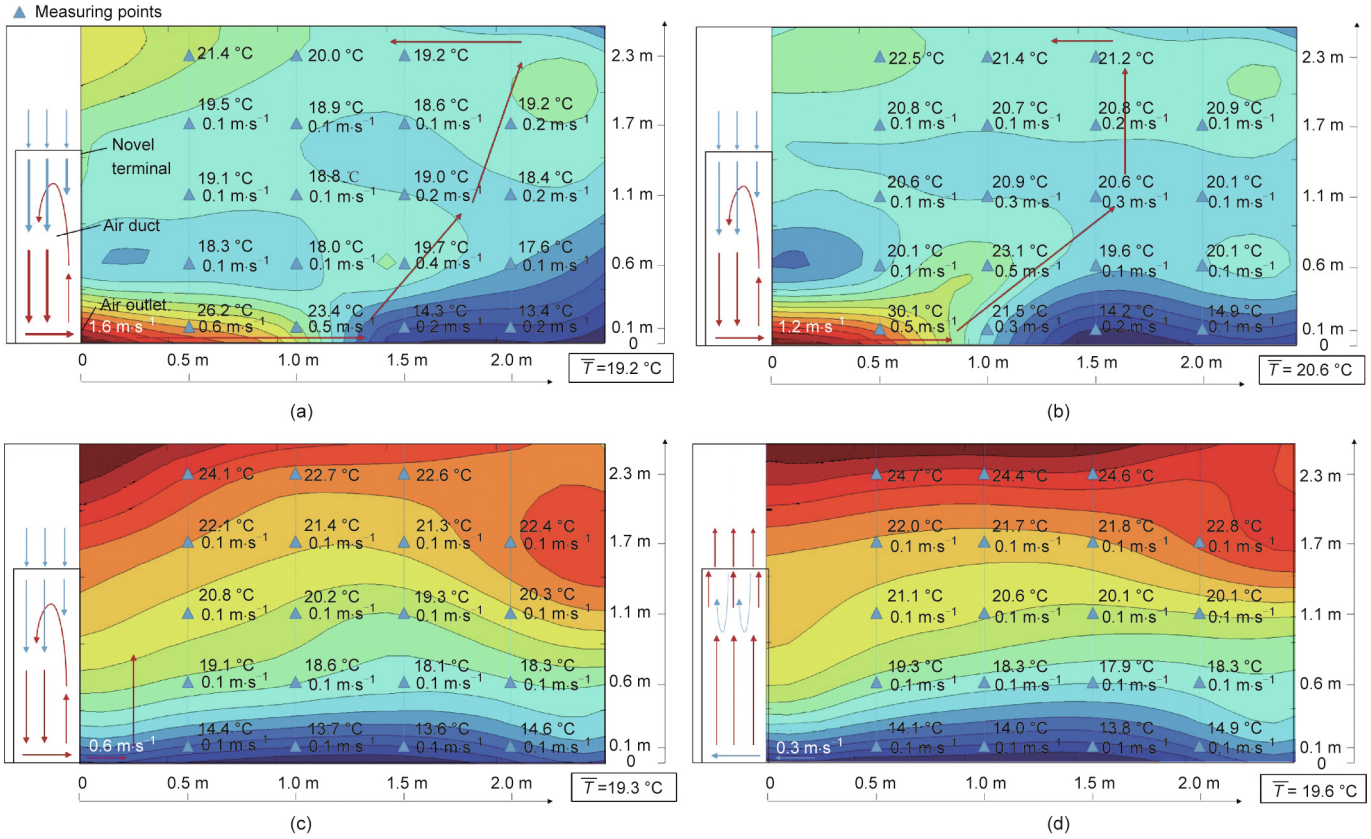

Fig. 17. Room temperature distribution under different forced convection wind speeds. Outlet wind speed: (a) nominal: 2.0 m·s^{-1}, actual: 1.6 m·s^{-1}; (b) nominal: 1.5 m·s^{-1}, actual: 1.2 m·s^{-1}; (c) nominal: 1.0 m·s^{-1}, actual: 0.6 m·s^{-1}; (d) nominal: 0 m·s^{-1}, actual: −0.3 m·s^{-1}. $\overline{T}$: average room temperature.

lower side. As the hot air rises and flows back, it provides a uniform temperature distribution in the area where personnel activity occurs (0.6–1.7 m). Similarly, Fig. 17(b) shows that when the calibrated outlet wind speed is 1.5 m·s^{-1}, the actual outlet wind speed is 1.2 m·s^{-1}. When compared with an outlet wind speed of 2.0 m·s^{-1}, the air supply reaches a shorter distance of approximately 1.0 m.

However, as shown in Fig. 17(c), there is a change in the room temperature distribution when the calibrated outlet wind speed is 1.0 m·s^{-1} but the actual outlet wind speed is 0.6 m·s^{-1}. The low outlet wind speed (0.2 m·s^{-1}) results in no noticeable draughts in the room; this not only enables uniformity in the indoor temperature but also eliminates draughts. In Fig. 17(d), the calibrated outlet wind speeds are 0.5 and 0 m·s^{-1}. The thermal buoyancy force is greater than the cross-flow fan power, therefore the reversed wind speed is 0.3 m·s^{-1}. There is a noticeable vertical temperature difference in this situation.

Figs. 17(a) and (b) illustrate the working conditions created by a lower-side heat source and lower-side air supply. As an example, at a distance of 1.0 m from the terminal, the maximum vertical temperature difference is 5.4 °C, leading to a differential thermal distribution that is characterized as "cold head and warm feet." The outlet wind speed can also be adjusted in this mode, and the space can be heated.

4.4. Comparison between the thermal performance of the novel terminal and existing heating terminals

A comparison with existing heating terminals is conducted in order to evaluate the thermal performance of the new terminal

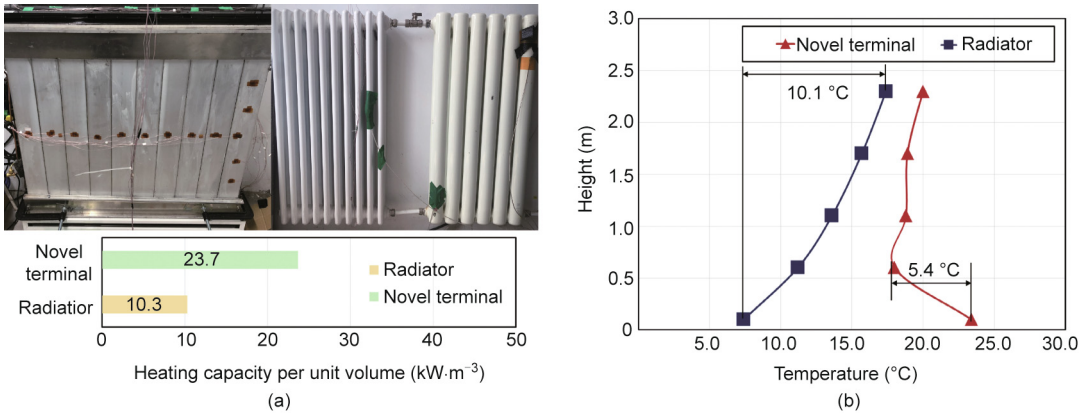

Fig. 18. Thermal performances of novel terminal and radiator: (a) heating capacity per unit volume and (b) room temperature distribution (at a distance of 1.0 m from the terminal).

effectively. An evaluation of a heating terminal should take into account not only its heating capacity but also the size of the space that it is required to heat. Therefore, the heating capacity per unit volume is compared. A typical heating terminal (a radiator) relies very much on radiation heat transfer to provide the major portion of its heat, and such terminals are widely used in space heating because of their thermal comfort and ease of installation. In addition, the size and shape of the radiator are similar to that of the novel terminal, which is selected for comparison.

To reveal the advantages of the reasonably high radiation heat transfer ratio of the radiator, its surface temperature (approximately 40 °C) and radiant area (approximately 0.85 m^2) are controlled in the experiment to be as close to those of the novel terminal as possible. Fig. 18 shows the heating capacity per unit volume and the room temperature distribution. The results show that the heating capacities per unit volume of the novel terminal and radiator are 23.7 kW·m^{-3} (98 cm × 88 cm × 10 cm) and 10.3 kW·m^{-3} (100 cm × 85 cm × 8 cm), respectively. Therefore, the heating capacity per unit volume of the novel terminal is 2.3 times higher than that of the radiator. Moreover, the maximum vertical temperature difference at 1.0 m away from the radiator is 10.1 °C, which is 1.9 times higher than that of the novel terminal (5.4 °C) under stable conditions. These results indicate that the novel terminal provides a larger heating capacity and better thermal comfort than the radiator.

Furthermore, the heating capacity per unit volume of the novel terminal is compared to that of the representative improved heating terminals [10,26,28], and their heating capacities per unit volume are shown in Fig. 19. The results show that the heating capacity per unit volume of the novel terminal is larger than the other terminals owing to the excellent heat transfer capacity of the thin FHP.

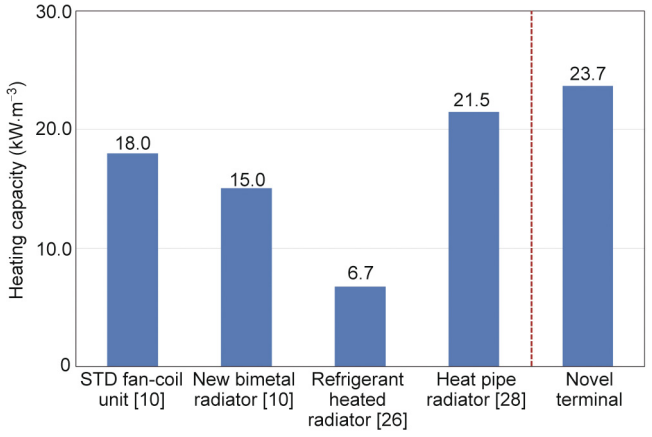

Fig. 19. Heating capacity per unit volume of different terminals. STD: small temperature difference.

4.5. Uncertainty analysis and thermal verification

Uncertainty analysis of the heating capacity is conducted based on the measured parameters and their accuracies (Table 3). The methods of Kline and McClintock [40] are used to describe the uncertainties, and the total uncertainties of the results are described by Eq. (10):

$$W_R = \left(\sum_{i=1}^{n} \frac{\partial R}{\partial v_n} W_{v_n} \right)^{1/2} \tag{10}$$

where R is the result obtained by calculation; v_n is the independent variable; W_{v_n} is the uncertainties about v_n; and W_R is the total uncertainties about R. Eq. (10) shows that the result (the heating capacity) is a function of several independent variables. Combined with Eq. (11), the uncertainty of the heat transfer coefficient can be expressed as

$$W_Q = \left[\left(\frac{\partial Q}{\partial G} W_G \right)^2 + \left(\frac{\partial Q}{\partial T_o} W_{T_o} \right)^2 + \left(\frac{\partial Q}{\partial T_i} W_{T_i} \right)^2 \right]^{1/2} \tag{11}$$

where W_{T_o} is the uncertainties about T_o; W_{T_i} is the uncertainties about T_i; W_G is the uncertainties about G; and W_Q is the total uncertainties about Q. The results show that the uncertainty of the heating capacity (W_Q/Q) is found to be in the range of 3.2%–12.5%, which is in agreement with the experimental results.

A thermal verification of the three modes is also conducted to verify the accuracy of the results, which can be seen in Fig. 20. In Table 6, the middle part of the stable stage (360–540 s) is presented to illustrate the specific thermal verification process applied to the three modes. The total heating capacity Q, radiation heating capacity Q_r, and convection heating capacity Q_c of the terminal can be calculated using Eqs. (1)–(8), where Q is the amount of heat transferred from the heat source to the terminal, and Q_r and Q_c are the amounts of heat transferred from the terminal to the room through radiation and convection, respectively. Considering that the heat storage of the terminal is negligible, Q (heat source to terminal) should theoretically be equal to $Q_r + Q_c$ (terminal to room). In order to verify the accuracy of the experimental results, Q and $Q_r + Q_c$ are compared, and the error range is found to be within ±10%, which can be considered reasonably accurate.

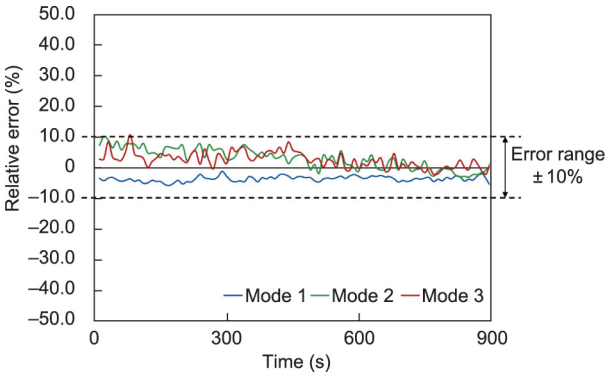

Fig. 20. Thermal verification of the three modes.

4.6. Limitations and future challenges

The results of this study show that the proposed radiation-adjustable heating terminal has a large heating capacity and rapid adjustability. Further, its improved structural design enables a more effective combination with ASHPs compared with the existing heating terminals. However, this study has certain limitations. First, the nominal heating capacity of the compressor limits its heating capacity. Increasing the maximum heating capacity could improve the thermal response of the compressor. As shown in Fig. 21, the outdoor unit is replaced to increase its nominal heating capacity from the original 2100 to 3600 W under the same conditions. The results showed that the maximum heating capacity and EER increased to 3540.1 W and 3.9, respectively. Second, the experiment is performed using R22 as the working medium due to its convenience. However, considering its environmental impact (R22: ozone depletion potential (ODP) = 0.055, global warming potential (GWP) = 1700), the use of an alternative working medium needs to be explored. Moreover, the climate of the experimental site, the size of experimental room, and the form of building envelope limited the indoor thermal load, so future experiments could be conducted with different indoor thermal loads. In addition, further research on the novel terminal may need to include an inverter compressor to enable local space heating and cooling during summer.

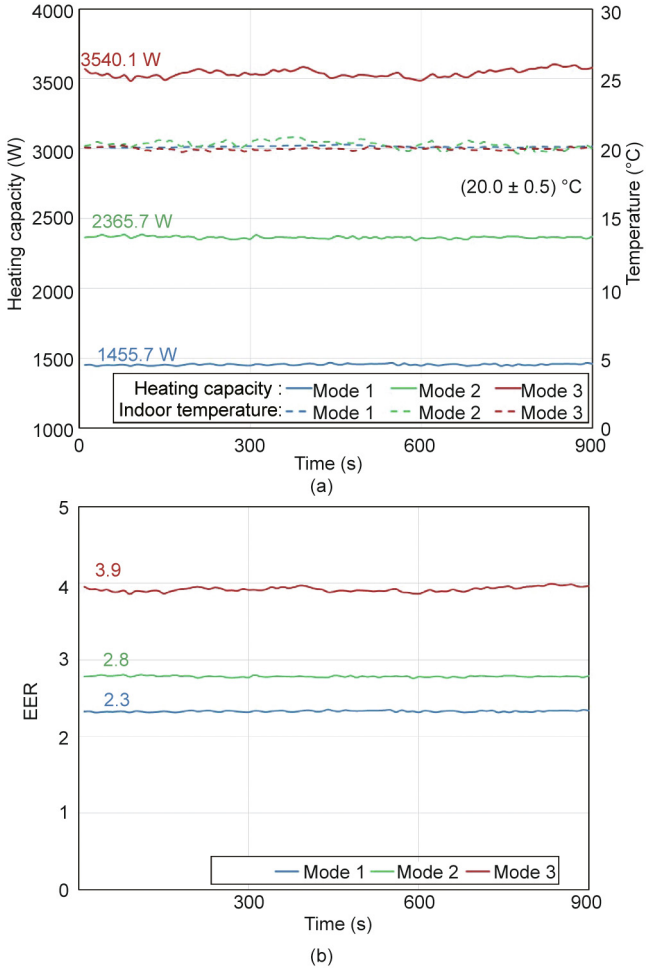

Fig. 21. Heating capacity and EER with a larger nominal heating capacity of the compressor: (a) heating capacity; and (b) EER.

5. Conclusions

This study presents a novel radiation-adjustable heating terminal with an ASHP primarily comprised of HEs and FHPs. The improved structural design of the terminal addresses three main issues associated with existing radiant terminals, namely, maximum heating capacity, adjustability, and the ability to connect it to an ASHP. The improvements in results were analyzed on the basis of maximum heating capacity, thermal response speed, and radiation heat transfer ratio, and the benefits of using an FHP to transfer heat from the drilled HE in combination with the ASHP were highlighted. Furthermore, a novel phased operation strategy for space heating using the novel terminal was proposed, and forced convection was added to the terminal to further enhance its adjustability for users. The notable conclusions are as follows:

(1) The structural design was improved by adding fins (Improvement A), adding cross-flow fans (Improvement B), and drilling the HE for refrigerant (Improvement D). With all modifications, the maximum heating capacity of the heating terminal was increased from 1649.9 to 2039.6 W, which represents a 23.6% in heating capacity.

Table 6
Thermal verification of the three modes (using the middle part of the stable stage at 420–480 s as an example).

Time (s)	Mode 1					Mode 2					Mode 3				
	Q_r (W)	Q_c (W)	$Q_r + Q_c$ (W)	Q (W)	Relative error	Q_r (W)	Q_c (W)	$Q_r + Q_c$ (W)	Q (W)	Relative error	Q_r (W)	Q_c (W)	$Q_r + Q_c$ (W)	Q (W)	Relative error
420	452	1245	1697	1659	−2.3%	284	1677	1962	2031	3.4%	196	1666	1862	1996	6.7%
430	452	1249	1701	1665	−2.1%	287	1664	1951	2035	4.1%	195	1697	1892	1986	4.7%
440	452	1248	1700	1655	−2.7%	288	1726	2014	2041	1.4%	196	1621	1817	1984	8.4%
450	452	1252	1704	1644	−3.6%	286	1690	1976	2041	3.2%	197	1672	1869	1983	5.8%
460	453	1250	1703	1654	−3.0%	287	1674	1961	2044	4.1%	196	1673	1869	1972	5.2%
470	453	1250	1703	1655	−2.9%	286	1674	1960	2044	4.1%	196	1696	1892	1986	4.7%
480	453	1253	1706	1652	−3.2%	288	1682	1970	2036	3.3%	196	1719	1915	1978	3.2%

Q_r: radiation heat transfer (from terminal to room); Q_c: convection heat transfer (from terminal to room); $Q_r + Q_c$: total heat transfer (from terminal to room); and Q: total heat transfer (from heat source to terminal).

(2) Improvement B (the addition of cross-flow fans) was useful for enhancing the rapid adjustability of the heating terminal. The time required for the indoor temperature to rise from an initial 7–8 to 18 °C was reduced from 5470 to 2410 s, and the radiation heat transfer ratio increased by 2.6 times. Consequently, forced convection provided users with more autonomy in adjustment with a radiation heat transfer ratio ranging from 10.1% to 30.9%.

(3) Improvement D (drilling the HE for refrigerant) and Improvement E (use of an FHP to transfer heat) ensured a better connection between the heating terminal and ASHP. As a result of the innovative design of the FHP, which takes its heat from the drilled HE, there was a considerable reduction in the exposed refrigerant pipe length in existing heating terminals. This solved the existing stability issues (compressor oil return), intermittent operation (refrigerant thermal inertia), and safety (risk of refrigerant pipe leakage) for existing terminals combined with ASHP.

(4) A phased operation strategy was proposed that divides the period of transition into two critical stages: a start-up period and a stabilization period. The heating mode at maximum heating capacity achieved the fastest thermal response during the starting period, and the heating mode with the maximum radiation heat transfer ratio provided the best thermal comfort during the stable period. Compared with existing heating terminals, the novel terminal provides comprehensive advantages with respect to heating capacity (23.7 $kW \cdot m^{-3}$) and thermal comfort (the vertical temperature difference produced by the radiator was 1.9 times greater).

In summary, the proposed novel heating terminal achieves improved heating performance compared to existing terminals and can be skillfully combined with an AHSP. The novel terminal makes use of FHPs, optimizes internal thermal resistance, and adds forced convection to provide a broad range of heating capacities, strong terminal adjustability, and a better combination of an ASHP with the terminal. The results of this study can be used as reference information for the electrification of heating terminals in order to achieve decarbonization of buildings.

Acknowledgments

The study was supported by the National Science Foundation for Distinguished Young Scholars of China (51825802).

Compliance with ethics guidelines

Yifan Wu, Hongli Sun, Mengfan Duan, Borong Lin, Hengxin Zhao, and Chaohung Liu declare that they have no conflict of interest or financial conflicts to disclose.

Nomenclature

A	surface area of radiant panel (m^2)
c	heat capacity of air, 1005 ($J \cdot kg^{-1} \cdot K^{-1}$)
G	flow rate of refrigerant ($kg \cdot h^{-1}$)
Gr	Grashof number
h_i	inlet enthalpy of terminal ($kJ \cdot kg^{-1}$)
h_o	outlet enthalpy of terminal ($kJ \cdot kg^{-1}$)
K	heat transfer coefficient ($W \cdot m^{-2} \cdot K^{-1}$)
K_n	natural convection heat transfer coefficient ($W \cdot m^{-2} \cdot K^{-1}$)
l	characteristic length (m^2)
Nu	Nusselt number
P	total electric power of compressor and fan (W)
P_i	inlet pressure of terminal (MPa)
P_o	outlet pressure of terminal (MPa)
Pr	Prandtl number
Q	heating capacity of terminal (W)
Q_c	convection heating capacity of terminal (W)
Q_f	forced convection heating capacity of terminal (W)
Q_n	natural convection heating capacity of terminal (W)
Q_r	radiation heating capacity of terminal (W)
R	the result obtained by calculation
Ra	Rayleigh number
T_a	ambient temperature (°C)
T_{exh}	exhaust temperature of compressor (°C)
T_i	air inlet temperature of terminal (°C)
T_o	air outlet temperature of terminal (°C)
T_s	surface temperature of terminal (°C)
V	forced convection wind speed ($m^3 \cdot s^{-1}$)
v_n	the independent variable
W_G	the uncertainties about G
W_Q	the total uncertainties about Q
W_R	the total uncertainties about R
W_{T_i}	the uncertainties about T_i
W_{T_o}	the uncertainties about T_o
W_{v_n}	the uncertainties about v_n
α	volume expansion coefficient (K^{-1})
σ_b	Stefan–Boltzmann constant, 5.67×10^{-8} ($W \cdot m^{-2} \cdot K^{-4}$)
β	radiation heat transfer ratio
ε	surface emissivity
ρ	density of air ($kg \cdot m^{-3}$)
λ	thermal conductivity of air ($W \cdot m^{-1} \cdot K^{-1}$)
υ	kinematic viscosity ($m^2 \cdot s^{-1}$)
ASHP	air source heat pump
EER	energy efficiency ratio
FHP	flat heat pipe
FMHPA	flat micro-heat pipe array
HE	heat exchanger
HVAC	heating, ventilation, and air conditioning
MRT	mean radiant temperature

References

[1] Cao X, Dai X, Liu J. Building energy-consumption status worldwide and the state-of-the-art technologies for zero-energy buildings during the past decade. Energy Build 2016;128:198–213.
[2] Building Energy Saving Research Center of Tsinghua University. Annual report on China building energy efficiency. Report. Beijing: China Architecture and Building Press; 2020. Chinese.
[3] Krausmann F, Wiedenhofer D, Haberl H. Growing stocks of buildings, infrastructures and machinery as key challenge for compliance with climate targets. Glob Environ Change 2020;61:102034.
[4] Sovacool BK, Cabeza LF, Pisello AL, Colladon AF, Larijani HM, Dawoud B, et al. Decarbonizing household heating: reviewing demographics, geography and low-carbon practices and preferences in five European countries. Renew Sustain Energy Rev 2021;139:110703.
[5] Romanchenko D, Nyholm E, Odenberger M, Johnsson F. Impacts of demand response from buildings and centralized thermal energy storage on district heating systems. Sustain Cities Soc 2021;64:102510.
[6] Bloess A, Schill WP, Zerrahn A. Power-to-heat for renewable energy integration: a review of technologies, modeling approaches, and flexibility potentials. Appl Energy 2018;212:1611–26.
[7] Thomaßen G, Kavvadias K, Jiménez Navarro JP. The decarbonisation of the EU heating sector through electrification: a parametric analysis. Energy Policy 2021;148(A):111929.
[8] Duan M, Wu Y, Sun H, Yang Z, Shi W, Lin B. Intermittent heating performance of different terminals in hot summer and cold winter zone in China based on field test. J Build Eng 2021;43:102546.
[9] Guo S, Yan D, Peng C, Cui Y, Zhou X, Hu S. Investigation and analyses of residential heating in the HSCW climate zone of China: status quo and key features. Build Environ 2015;94(2):532–42.
[10] Hu B, Wang RZ, Xiao B, He L, Zhang W, Zhang S. Performance evaluation of different heating terminals used in air source heat pump system. Int J Refrig 2019;98:274–82.
[11] Hemadri VA, Gupta A, Khandekar S. Thermal radiators with embedded pulsating heat pipes: infra-red thermography and simulations. Appl Therm Eng 2011;31(6–7):1332–46.

[12] Wang D, Wu C, Liu Y, Chen P, Liu J. Experimental study on the thermal performance of an enhanced-convection overhead radiant floor heating system. Energy Build 2017;135:233–43.
[13] Chae YT, Strand RK. Thermal performance evaluation of hybrid heat source radiant system using a concentrate tube heat exchanger. Energy Build 2014;70:246–57.
[14] Li T, Liu Y, Chen Y, Wang D, Wang Y. Experimental study of the thermal performance of combined floor and Kang heating terminal based on differentiated thermal demands. Energy Build 2018;171:196–208.
[15] Li Z, Zhang D, Li C. Experimental evaluation of indoor thermal environment with modularity radiant heating in low energy buildings. Int J Refrig 2021;123:159–68.
[16] Zhao M, Gu ZL, Kang WB, Liu X, Zhang LY, Jin LW, et al. Experimental investigation and feasibility analysis on a capillary radiant heating system based on solar and air source heat pump dual heat source. Appl Energy 2017;185:2094–105.
[17] Ding P, Li Y, Long E, Zhang Y, Liu Q. Study on heating capacity and heat loss of capillary radiant floor heating systems. Appl Therm Eng 2020;165:114618.
[18] World bank group climate change action plan 2016–2020. Report. Washington, DC: World Bank; 2017.
[19] Grafakos S, Viero G, Reckien D, Trigg K, Viguie V, Sudmant A, et al. Integration of mitigation and adaptation in urban climate change action plans in Europe: a systematic assessment. Renew Sustain Energy Rev 2020;121:109623.
[20] Calderón C, Underwood C, Yi J, Mcloughlin A, Williams B. An area-based modelling approach for planning heating electrification. Energy Policy 2019;131:262–80.
[21] Carroll P, Chesser M, Lyons P. Air source heat pumps field studies: a systematic literature review. Renew Sustain Energy Rev 2020;134:110275.
[22] Vorushylo I, Keatley P, Shah N, Green R, Hewitt N. How heat pumps and thermal energy storage can be used to manage wind power: a study of Ireland. Energy 2018;157:539–49.
[23] Xiao B, He L, Zhang S, Kong T, Hu B, Wang RZ. Comparison and analysis on air-to-air and air-to-water heat pump heating systems. Renew Energy 2020;146:1888–96.
[24] Lin B, Wang Z, Sun H, Zhu Y, Ouyang Q. Evaluation and comparison of thermal comfort of convective and radiant heating terminals in office buildings. Build Environ 2016;106:91–102.
[25] Yoshino H, Guan S, Lun YF, Mochida A, Shigeno T, Yoshino Y, et al. Indoor thermal environment of urban residential buildings in China: winter investigation in five major cities. Energy Build 2004;36(12):1227–33.
[26] Shao S, Zhang H, You S, Zheng W, Jiang L. Thermal performance analysis of a new refrigerant-heated radiator coupled with air-source heat pump heating system. Appl Energy 2019;247:78–88.
[27] Dong J, Zhang L, Deng S, Yang B, Huang S. An experimental study on a novel radiant-convective heating system based on air source heat pump. Energy Build 2018;158:812–21.
[28] Xu S, Ding R, Niu J, Ma G. Investigation of air-source heat pump using heat pipes as heat radiator. Int J Refrig 2018;90:91–8.
[29] Yang B, Dong J, Zhang L, Song M, Jiang Y, Deng S. Heating and energy storage characteristics of multi-split air source heat pump based on energy storage defrosting. Appl Energy 2019;238:303–10.
[30] Zhang H, Jiang L, Zheng W, You S, Jiang T, Shao S, et al. Experimental study on a novel thermal storage refrigerant-heated radiator coupled with air source heat pump heating system. Build Environ 2019;164:106341.
[31] Wang T, Zhao Y, Diao Y, Ma C, Zhang Y, Lu X. Experimental investigation of a novel thermal storage solar air heater (TSSAH) based on flat micro-heat pipe arrays. Renew Energy 2021;173:639–51.
[32] Weng C, Wang Z, Xiang J, Zhao X, Chen F, Zheng S, et al. Numerical and experimental investigations of the micro-channel flat loop heat pipe (MCFLHP) heat recovery system for data centre cooling and heat recovery. J Build Eng 2021;35:102088.
[33] Jouhara H, Almahmoud S, Chauhan A, Delpech B, Bianchi G, Tassou SA, et al. Experimental and theoretical investigation of a flat heat pipe heat exchanger for waste heat recovery in the steel industry. Energy 2017;141:1928–39.
[34] Tan R, Zhang Z. Heat pipe structure on heat transfer and energy saving performance of the wall implanted with heat pipes during the heating season. Appl Therm Eng 2016;102:633–40.
[35] Xin F, Ma T, Wang Q. Thermal performance analysis of flat heat pipe with graded mini-grooves wick. Appl Energy 2018;228:2129–39.
[36] Sun H, Wu Y, Lin B, Duan M, Lin Z, Li H. Experimental investigation on the thermal performance of a novel radiant heating and cooling terminal integrated with a flat heat pipe. Energy Build 2020;208:109646.
[37] Li J, Li X, Zhou G, Liu Y. Development and evaluation of a supersized aluminum flat plate heat pipe for natural cooling of high power telecommunication equipment. Appl Therm Eng 2021;184:116278.
[38] Wu Y, Sun H, Duan M, Lin B, Zhao H. Dehumidification-adjustable cooling of radiant cooling terminals based on a flat heat pipe. Build Environ 2021;194:107716.
[39] Song Z, Ji J, Cai J, Li Z, Han K. Performance analyses on a novel heat pump with a hybrid condenser combined with flat plate micro-channel heat pipe plus TEG and FPV evaporator. Energy Convers Manage 2021;228:113606.
[40] Kline SJ, McClintock FA. Describing uncertainties in single sample experiments. Mech Eng 1953;75:3–8.